International Journal of Pharmaceutics: X 6 (2023) 100201

Contents lists available at ScienceDirect

International Journal of Pharmaceutics: X

journal homepage: www.sciencedirect.com/journal/international-journal-of-pharmaceutics-x

Spanlastic-laden in situ gel as a promising approach for ocular delivery of Levofloxacin: In-vitro characterization, microbiological assessment, corneal permeability and in-vivo study

Omnia Ahmed Agha [a,*], Germeen N.S. Girgis [a], Mohamed M.A. El-Sokkary [b], Osama Abd El-Azeem Soliman [a]

[a] Department of Pharmaceutics, Faculty of Pharmacy, Mansoura University, Mansoura, Daqahlia 35516, Egypt
[b] Department of Microbiology and Immunology, Faculty of Pharmacy, Mansoura University, Mansoura, Daqahlia 35516, Egypt

ARTICLE INFO

Keywords:
Levofloxacin
Spanlastic
Sustained ocular delivery
Factorial design
Antibacterial activity
Confocal laser scanning

ABSTRACT

The objective of this study was to encapsulate the antibacterial drug levofloxacin hemihydrate (LF) into spanlastics (SLs) followed by incorporation into gelrite in situ gel to enhance its antibacterial activity and sustain ocular delivery. A combination of Span 60 as main vesicle component and Tweens as an edge activator (EA) was used to prepare SLs using the thin film hydration method. A 3^2 factorial design was applied to study the effect of formulation variables (ratio of Span 60: EA and type of EA) on SLs characteristics (encapsulation efficiency (EE %), particle size (PS), zeta potential (ZP) and percentage of drug released). In-vitro antimicrobial study was conducted to determine the antibacterial activity of the optimized formula. Finally confocal laser scanning microscopy (CLSM) was applied to monitor SLs corneal penetration. The optimum formulation (F5), contains 240 mg Span 60 and 60 mg Tween 60 as EA. F5 exhibited EE% = 59.7 ± 4.2%, PS = 177.6 ± 1.8 nm, PDI = 0.27 ± 0.022 and ZP = -40.6 ± 0.68 mV. Furthermore, only 39.37 ± 0.72% of LF amount was released after 4 h compared to complete release from drug solution. The apparent permeation coefficient was (14.7×10^{-3} cm/h) compared to (9.7×10^{-3} cm/h) for LF solution. Moreover, F5 exhibited 200% and 100% increase in the antibacterial efficacy against *Pseudomonas aeruginosa* and *Staphylococcus aureus* respectively.

1. Introduction

Many of eye problems are associated with bacterial infections such as conjunctivitis, blepharitis, endophthalmitis and keratitis. They considered a real threat to eye if left untreated as they can progress to blindness so an immediate and proper management is required (Saher et al., 2016a). Acute bacterial infection is commonly treated by topical flouroquinolones.

Levofloxacin (LF) is a synthetic third generation fluoroquinolones. It's the L-isomer of ofloxacin with broad spectrum antibacterial effect against both gram negative and gram positive bacteria (Noel, 2009) by inhibiting DNA gyrase and topoisomerase IV (Hooper, 1999). In case of topical application, it provides effective antibacterial effect on cornea with frequent administration about every 1–2 h for first 3 days then every 4–5 h (Ameeduzzafar Imam et al., 2018) so trials to attain sustained release dosage form can be advantageous.

One of main drawbacks of topically applied conventional ocular delivery systems is the extensive and rabid loss of drug due to the nasolacrimal drainage and high tear fluid turnover (Bourlais et al., 1998). Researches previously made efforts to enhance the penetration of drugs through the cornea and extend their duration of action by employing various nanosystems like nanoparticles, nanoemulsions, niosomes, liposomes and cubosomes. These nanosystems have proved to improve the therapeutic efficacy by effectively encapsulating the drugs.

Abbreviations: CLSM, Confocal Laser Scanning Microscopy; DSC, Differential Scanning Calorimetry; EA, Edge Activator; EE%, Entrapment Efficiency; FT-IR, Fourier-Transform Infrared Spectroscopy; HLB, Hydrophilic Lipophilic Balance; LF, Levofloxacin hemihydrate; LSG, Levofloxacin spanlastic laden in situ gel; MIC, Minimum Inhibition Concentreation; MBC, Minimum Bactericidal Concentration; PS, Particle Size; PDI, Polydispersity Index; RhB, Rhodamine B; $R_{4h\%}$, $R_{24h\%}$, Percentage of drug released after 4, 24 h; rpm, Rotation per minute; r^2, Correlation Coefficient; SL, Spanlastic; STF, Simulated Tear Fluid; TEM, Transmission Electron Microscopy; XRD, X-ray Diffractometry; ZP, Zeta Potential.

* Corresponding author at: Department of Pharmaceutics, Faculty of Pharmacy, Mansoura University, El-Gomhoria Street, Mansoura, Daqahlia 35516, Egypt.
E-mail address: Omnia.agha@mans.edu.eg (O.A. Agha).

https://doi.org/10.1016/j.ijpx.2023.100201
Received 8 June 2023; Received in revised form 9 July 2023; Accepted 23 July 2023
Available online 24 July 2023

A number of strategies for ocular delivery of LF using nanocarriers were developed such as PLGA nanoparticles (Gupta et al., 2011), chitosan nanoparticles (Ameeduzzafar Imam et al., 2018), nanospheres (De Gaetano et al., 2021), solid lipid nanoparticles (Baig et al., 2016), nanoemulgel (Mehanna et al., 2020) and proniosomes (Dhangar et al., 2014).

Recently, spanlastics (SLs) have been developed, a surfactant based nanovesicular elastic carrier system, composing of Span 60 and Tween 80 as non-ionic surfactant for vesicle formation, and an edge activator (EA) respectively. The addition of EA has imported elasticity to vesicles to overcome the rigidity of niosomes so improving the penetration across different tissues. Researchers previously employed SLs to improve both corneal permeation and skin delivery of different drugs (Kakkar and Kaur, 2011) and hence it can be promising approach for ocular delivery of LF.

Ocular in situ gels are valuable dosage forms for ocular delivery. They allow for prolonging ocular contact time, decreasing nasolacrimal drainage and hence decreasing dose frequency. In situ gels differ from gels in their nature as they present in liquid state which provides ease of administration and undergo phase transition to solid state upon contact with tear fluids in response to different stimuli depending on their mechanism of action (Kumar et al., 1994).

The aim of current study is to formulate LF in dosage form that combines advantages of both nano-systems (SLs) and insitu gels as a promising tool for sustained delivery, enhanced antimicrobial activity and improved LF penetration across the cornea.

2. Materials

Levofloxacin hemihydrate was kindly received as gift sample from Amoun Pharmaceutical Co., Cairo, Egypt. Rhodamine B (RhB) as a fluorescent marker was purchased from Alpha Aesar, Germany. Sorbitan monostearate (Span 60) was purchased from Piochem, Egypt. Polyoxyethylene sorbitan monooleate (Tween 80) and Polyoxyethylene sorbitan monolaurate (Tween 20) were obtained from Adwic, El-Nasr Pharmaceutical Chemicals Co., Egypt. Polyoxyethylene sorbitan monostearate (Tween 60) was purchased from Sisco Research Laboratories, India. Millipore filter (0.45 μm) was purchased from Cornell lab (Cairo, Egypt). Gelrite was acquired from LANXESS Company, Germany. NaCl, $NaHCO_3$ and $CaCl_2{\cdot}2H_2O$ were purchased from El-Nasr Pharmaceutical Chemicals Co., Egypt. Methanol and absolute ethanol were purcahsed from Fisher Scientific, UK.ce.

3. Methodology

3.1. Preparation of levofloxacin loaded spanlastics (LF-SLs)

SLs were prepared by thin film hydration method (Al-Mahallawi et al., 2017). Nine formulations were prepared according to 3^2 factorial design as indicated in Table 2. Span 60 used as the main vesicle forming component with different grades of Tween as an EA at different weight ratios of 9:1, 8:2, and 7:3 (total weight 300 mg was chosen based on preliminary trials).

To prepare the SLs, first, a precise amount of Span 60 was weighed and dissolved in 10 mL of absolute ethanol in a well closed tube using a bath sonicator (Sonix IV, SS101H230, USA) until a clear solution was obtained. The resulting solution was then transferred into a round bottom flask and the organic solvent was removed under vacuum using a rotary evaporator (Wheaton, Chicago, Illinois, USA) at 60 °C to create a thin film on the walls of the flask. Subsequently, the thin film was hydrated by adding an aqueous phase consisting of 20 mg LF and a specific amount of EA dissolved in 7.5 mL deionized water. The flask was then rotated in a water bath at 100 rpm for 1 h at the same temperature under normal pressure. Finally, the resulting suspension was bath sonicated for 3 min to reduce the particle size (Shamma and Elsayed, 2013). The resulting dispersion was then stored at4 °C to allow for maturation and further analysis.

3.2. Characterization of prepared SLs

3.2.1. Entrapment efficiency % (EE %)

To determine the total drug content (TD) of the prepared formulations, a specific volume of the dispersion was dissolved in hot ethanol to disrupt the dispersed vesicles. After being properly diluted, the resulting solution was filtered through 0.45 μm Millipore filter and the absorbance was measured at a predetermined λ_{max} of 286 nm (Saher et al., 2016a) using a UV spectrophotometer (model UV-1601 PC, Shimadzu, Kyoto, Japan). Free drug was separated from the vesicular system by centrifugation at 16000 rpm and 4 °C for 3 h using a cooling centrifuge (Acculab 16CE-4X100RD, USA). Then supernatant removed, filtered, properly diluted with deionized water and measured spectrophotometrically to determine free LF (FD). Plain SLs were prepared and treated in the same manner to be used as blank. Experiments were repeated in triplicates and %EE was calculated indirectly from the following eq.

$$EE\% = \frac{TD - FD}{TD} \times 100 \quad (1)$$

3.2.2. Determination of particle size (PS), zeta potential (ZP) and polydispersity index (PDI)

All prepared formulations (F1-F9) were properly diluted (1:100) by deionized water for measuring size, PDI in addition to ZP using Malvern zeta sizer (Nano ZS 90, Malvern, UK). Each measurement repeated triplicate at 25 °C.

3.2.3. In-vitro release study of LF from prepared SLs

The in-vitro release of LF from pthe repared formulations was conducted in GFL shaking water bath (GFL, Gesellschaft fur Labortechnik GmbH, Burgwedel, Germany) using modified Franz diffusion cell representing donor compartment. Cells were tightly covered with semipermeable cellophane membrane which was previously soaked overnight in simulated tear fluid (STF), which was prepared by mixing NaCl (0.68 g), $NaHCO_3$ (0.22 g), $CaCl_2{\cdot}2H_2O$ (0.008 g), and distilled water to a final volume of 100 mL. The freshly prepared STF at pH of 7.4 was used as the release media to simulate the physiological conditions.

SLs suspensions were centrifuged to remove free drug, cake dispersed in water and 50 μL of the dispersion was assayed for drug content after dissolving in absolute ethanol. Certain volume of each formula equivalent to 2 mg of LF was accurately measured and carefully placed on membrane surface of the donor chamber. Cell was suspended in a 250 mL beaker containing 50 mL of release media (representing receptor compartment) so cell just touching the media. The receptor cell was maintained at 37 ± 0.5 °C and continuously stirred at 50 rpm.

At predetermined time intervals up to 24 h, 1 mL sample was withdrawn and replaced with an equal volume of fresh media to maintain sink condition. Aliquots were diluted and analyzed spectrophotometrically to determine the amount of drug released. Each measurement repeated triplicate.

3.2.4. Release kinetics

GraphPad Prism software (version 6.00; Graphpad Software, San Diego, CA, USA) was utilized to analyze the kinetics data obtained from different formulations release. Generally, the data was adjusted to different release models such as zero-order, first-order (Martin et al., 1993), and higuchi models (Higuchi, 1963) to show which model is best representative to LF release. The pattern of LF release from formulations was attained by the model with the highest correlation coefficient (r^2). Also Korsmeyer–Peppas kinetic model was applied to predict the main transport mechanism (Korsmeyer et al., 1983).

3.2.5. Statistical Analysis

A complete 3^2 factorial design was conducted using Design-Expert®

software (Stat-Ease, Inc., Minneapolis, Minnesota, USA) and employed for optimizing the formulation variables. Two factors, each with 3 levels, were studied: EA Type (X1) and Span 60: EA ratio (*w*/w) (X2). Table 1 summarizes the design. The experimental results were analyzed and formulation with the highest desirability was selected as the optimum one (Abdelbari et al., 2021).

3.3. Characterization of the optimum LF-SL (F5)

Regarding the obtained results, F5 (consists of Span 60: Tween 60 at 80: 20 weight ratio) was chosen as the optimum formula and hence was subjected for further investigation and incorporation in the final dosage form.

3.3.1. Transmission electron microscopy (TEM)

The morphological examination of the optimum LF-SL suspension (F5) was conducted using TEM (JEM-2000EX II, JEOL, Tokyo, Japan). A drop of the sample was properly diluted and fixed onto the surface of a carbon-coated copper grid. The vesicles were then negatively stained with a 2% (*w/v*) aqueous solution of phosphotungstic acid for 5 min, air-dried for 10 min at room temperature, and finally microscopically examined (Abdelbary et al., 2016).

3.3.2. Solid state characterization

The un-entrapped LF was separated from (F5) vesicles through ultra-centrifugation as discussed before. The sediment was dispersed in water, frozen and subjected to lyophilization. Plain F5 was treated in the same manner and the resulting lyophilized vesicles, as well as the physical mixture and the individual components, were investigated through the following solid-state examinations (Tayel et al., 2015).

3.3.2.1. Fourier-Transform Infrared Spectroscopy (FT-IR Spectroscopy). FT-IR spectral analysis of LF, Span 60, Tween 60, their corresponding physical mixture, plain and LF loaded (F5) freeze-dried samples were conducted by FT-IR spectroscopy (Thermo Fisher Scientific iS10 Nicolet) to assess any possible interactions between different system components. Samples were mixed and finely grounded with potassium bromide then pressed into KBr disks to be scanned. The scanning limit ranged from 500 to 4000 cm^{-1}.

3.3.2.2. Differential Scanning Calorimetry (DSC). DSC (Shimadzu DSC 50, Tokyo, Japan) was applied for thermal analysis of the samples to assess any changes in thermograms of the different ingredients and any possible interactions between them. Samples were heated from 25 °C to 400 °C in aluminum pans at a rate of 10 °C per minute under a dry nitrogen flow of 20 mL/min (ElMeshad and Mohsen, 2016).

3.3.2.3. X-Ray Diffractometry (XRD). The degree of crystallinity of different components before and after being formulated was assessed by using X-ray diffractometer with Cu-Kα radiation (Rigaku Rint-2500VL, Tokyo, Japan) (Singh et al., 2019). Samples of LF, Span 60, physical mixture, medicated and plain F5 freeze-dried samples were investigated.

Table 1
The independent variables levels used to formulate LF-SLs.

Factors (Independent variables)	Levels		
X_1: (Type of EA)	Tween 80 (−1)	Tween 60 (0)	Tween 20 (1)
X_2: (Span 60: EA ratio (w/w)	90:10 (−1)	80:20 (0)	70:30 (1)
Responses (Dependent Variables)	Desirability Constraints		
Y_1: EE%	Maximize		
Y_2: PS (nm)	Minimize		
Y_3: PDI	Minimize		
Y_4: ZP (mV)	Maximize (absolute value)		
Y_5: R_{4h}%	Minimize		
Y_6: R_{24h}%	Minimize		

3.4. Ex-vivo corneal permeability study

Membrane diffusion technique was applied to study the Ex-vivo corneal permeability across freshly excised rabbit cornea. Same as in-vitro release, the studies were conducted within a vertical Franz cell using GFL shaker maintained at a constant temperature (37±1 °C) and 100 rpm.

The excised cornea was mounted between the donor and the receptor compartments. Both LF solution and F5 dispersion (equivalent to 1 mg LF) were placed in the donor compartment on the corneal epithelium. The receptor media was 25 mL of freshly prepared STF pH 7.4. A plain dispersion was treated with the same manner to be used as blank and avoid any possible interference. At fixed time intervals, 1 mL aliquot was withdrawn and replaced with fresh medium to maintain a constant volume. The samples were analyzed spectrophotometrically, and the experiment was repeated triplicate to calculate the mean ± SD. The following equation was used to calculate the apparent permeability coefficient (Papp).

$$\text{Papp} = \frac{\Delta Q}{\Delta t} \times \frac{1}{(A.C_{\circ})} \quad (2)$$

Where ΔQ/Δt (μg/h) is the flux across the corneal tissue, $C_{\circ}$ (μg/mL) is the initial concentration of drug in the donor compartment and A is the area of diffusion (cm^2). The flux was calculated from the slope of the linear portion of the curve between the amount permeated (Q) versus time (t).

3.5. Formulation of LF-SL laden in situ gel (LSG)

Accurately weighed amounts of gelrite dissolved in deionized water at 50° c with stirring at 600 rpm to prepare plain ion activated in situ gel in different concentrations from 0.1% to 0.5% *w/v*. The optimum formula F5 was ultra-centrifuged to remove the un-entrapped drug and the residue was uniformly dispersed in the polymer solution.

3.6. Characterization of LSG

3.6.1. Gelling capacity

To determine the gelling capacity of formulations, a small amount (100 μL) of the formulation was added to a test tube containing 2 mL of freshly prepared STF solution. The time required for the gelation to start and time the gel took to be completely dissolved was observed (Alsaidan et al., 2022).

3.6.2. pH and rheological properties

Digital pH meter (Beckman Instruments Fullerton, CA 92634, Germany) was used to determine pH of the prepared formulations, and viscosity of formulations before and after gelation was measured by Brooke field viscometer (Haake Inc., Germany) at room temperature. All measures were done in triplicate.

3.6.3. Drug content

One gram of the preparation was dissolved in hot ethanol with aid of sonication to completely disrupt the vesicles then filtered using 0.45 μm milipore filter, properly diluted and finally measured spectrophotometrically to determine amount of drug.

3.6.4. In-vitro drug release

LF release from both LSG in comparison with LF in situ gel as control was conducted in the same manner discussed above.

3.7. Microbiological study of optimum F5

The minimum inhibition concentration (MIC) was determined by the broth microdilution technique to compare the antibacterial activity of the optimized (F5), plain formula and marketed product (LF solution) against *S. aureus* and *P. aeruginosa* (Kahlmeter et al., 2003). In this study, Muller-Hinton Broth (Oxoid) was placed in a 96-well microtiter plate (Corning Incorporated, Corning, USA) and serial dilutions of LF solution, optimized F5, and plain F5,ranging from 500 to 4.76 $\times$ 10^{-4} µg/mL, were prepared and added to 20 wells. The wells were inoculated with 1 $\times$ 10^{6} colony forming units per milliliter (cfu/mL) of each organism, and the microtiter plate was incubated for 24 h at 37 °C, after which microbial growth was visualized (Abdelrahman et al., 2015).

The MIC is the minimum concentration that inhibited the microbial growth and determined by last clear tube. However, the MBC is the lowest concentration that kills at least 99.9% of the initial bacterial inoculum and determined by subculturing the last three clear tubes -with no observed growth in MIC assay- on Muller-Hinton agar medium and checking for absence of growth.

3.8. Stability study

The stability of the optimum (F5) dispersion was monitored by storing at two different temperatures (−4 °C in a refrigerator and 25 ± 2 °C) over a period of 3 months. Samples were collected at intervals of 1, 2, and 3 months and assessed for any physical changes in color or odor, PS, PDI, ZP, and % EE. Triplicate measurements were taken for each parameter and the mean value was calculated. Statistical analysis was performed using ANOVA test followed by Tukey-Kramer multiple comparisons test with Graphpad prism software (version 5.00; San Diego, CA, USA), at a significance level of $\rho < 0.05$.

3.9. In-vivo study

Ocular irritation and corneal penetration studies were conducted in accordance with the ARRIVE guidelines and approved by the Research Ethics Committee of the Faculty of Pharmacy at Mansoura University, Egypt. Adult male New Zealand albino rabbits, weighed approximately 2–3 kg each were used for studies. Animals were housed individually under standard environmental conditions, including a 12-h dark: light cycle, temperature of 20–25 °C, and relative humidity of 40–70%. They were fed with standard pellet diet and provided with water. Prior to the experimental study, all rabbits were examined and found to be healthy without any observable ocular abnormalities.

3.9.1. Eye irritation test

The study was conducted following the modified Draize test (Draize et al., 1944), and all glassware used in the experiment was sterilized by autoclaving. Nine New Zealand albino rabbits were used for the test and divided into three groups, with three rabbits in each group. The first group received plain F5 while the second and third groups received F5 and F5 loaded in situ gel respectively.

Two drops (100 µL) of each formulation was instilled into the lower cul-de sac of the right eye of each rabbit, while their left eye received saline and act as control. To minimize the loss of instilled preparations, the eyelids were gently held together for approximately 10 s. Animals were monitored for any ocular irritation reactions such as discharge, redness, conjunctival chemosis, iris or corneal lesions, immediate and 1, 6, 12, 24, 48, and 72 h after instillation (ElMeshad and Mohsen, 2016).

3.9.2. Corneal penetration study by confocal laser scanning microscopy (CLSM)

CLSM technique was applied to investigate the ability of the formulated SL system (F5) to enhance the penetration of the tested drug across corneal tissues in comparison to conventional eye drop. The monitoring of labeled formulation was done by inverted CLSM (LSM 710; Carl Zeiss, Jena, Germany) (Elsayed and Sayed, 2017).

First of all, F5 was prepared in the same manner mentioned above with the replacement of LF with 0.02% *w*/w Rhodamine B (RhB) as a fluorescent dye. The RhB loaded formulation was applied to the eye of male albino rabbit and contrasted to RhB solution at the same concentration (50 µl was applied twice with 5 min interval). After 6 h animals were sacrificed, eyes enuculated and transparent cornea carefully separated, rinsed, saved in artificial tears and photographed on the same day with CLSM without any further tissue processing. RhB was visualized by excitement at 485 nm and 595 nm using argon and helium-neon lasers, respectively. The cornea was scanned in the xy and xz directions using the z-stack mode, starting from its outer surface until the disappearance of RhB distinctive color. The acquired confocal images were analyzed with LSM software version 4.2 (Carl Zeiss Microimaging, Jena, Germany) (Sayed et al., 2020).

4. Results and discussion

4.1. Analysis of factorial design

To study the impact of certain variables on the characteristics of prepared SL formulations, a full factorial design was applied and analyzed statistically (Araújo et al., 2010). Nine experimental formulations (F1-F9) that combining two factors with three levels were formulated and studied. Table 2 below displays the independent variables and measured responses for all SLs formulations. See Fig. 1

Adequate precision, which is the ratio between signal and noise, was desired to be >4, and this acceptable ratio was achieved for all responses studied, as shown in Table 3. Additionally, the quality of the model was determined by the predicted R^2 value, which must be in rational agreement with the adjusted R^2 value and that was achieved for all responses studied as represented in Table 3.

4.1.1. Effect of formulation variables on the EE%

According to obtained statistical results it was obvious that both EA type (X1) and ratio (X2) had significant effect on the amount of LF entrapped within the vesicles ($p < 0.0001$) where the entrapment ranged from 22.45% to 67.4%.

Regarding the EA type, higher entrapment observed in case of Tween 80 and Tween 60 compared to Tween 20 this could be due to higher HLB value of Tween 20 (16.7) than Tween 60 and Tween 80 (15 and 14.9 respectively) as lower HLB value indicates higher hydrophobicity, decreasing fluidity and hence increasing overall entrapment % by increasing the membrane integrity (Moawad et al., 2017; Guinedi et al., 2005).

With respect to Span 60: EA ratio, the entrapment was inversely proportional to amount of EA where highest EE % was found in case of (90:10% *w*/w) Span 60: EA ratio regardless of EA type. Increasing EA% from 10% to 20% was accompanied by subsequent decreasing in the EE % and further increase to 30% resulted in the lowest EE% which in agreement with previous study (Moawad et al., 2017). This could be explained by the effect of EA on increasing the bilayer membrane fluidity with higher levels that meant increasing hydrophilic pores through which the entrapped drug might escape and hence reduce EE% (Duangjit et al., 2011).

4.1.2. Effect of formulation variables on the PS and PDI

The PS of all prepared SLs was <1 µm (nanoscale range) and ranged from 176 to 470.7 nm (Fig. 3A) which considered suitable for ocular delivery (Janoria et al., 2007) due to decreased eye irritation and increased bioadhesion (Yoncheva et al., 2005). Statistical analysis revealed that both design factors EA type (X1) and Span 60: EA ratio (X2) had significant effect on obtained vesicles size and PDI.

Regarding X1, Tween 80 formed the smallest vesicles while Tween 20 showed the largest one which in agreement with previous study which supposed that the use of surfactant with higher hydrophobicity

Table 2
Measured Responses of LF-SLs. Each value represents the mean ± SD ($n = 3$).

Code	Span 60:EA Ratio (X_1)	EA Type (X_2)	%EE Y_1	PS (nm) Y_2	PDI Y_3	ZP Y_4	R_{4h} (%) Y_5	R_{24h} (%) Y_6
F1*	9:1	Tw 80	63.50 ± 4.1	307.3 ± 7.10	0.55 ± 0.036	−42.3 ± 1.1	51.52 ± 1.10	91.66 ± 1.00
F2*	8:2	Tw 80	50.10 ± 2.9	176.0 ± 1.34	0.28 ± 0.032	−37.3 ± 0.49	54.23 ± 1.53	91.93 ± 1.53
F3*	7:3	Tw 80	25.30 ± 3.7	235.0 ± 3.70	0.43 ± 0.021	−38.1 ± 1.34	57.20 ± 1.53	91.40 ± 1.10
F4*	9:1	Tw 60	67.40 ± 2.5	437.6 ± 6.30	0.26 ± 0.049	−41.4 ± 1.16	43.95 ± 2.03	71.72 ± 1.70
F5*	8:2	Tw 60	59.70 ± 4.2	177.6 ± 1.80	0.27 ± 0.022	−40.6 ± 0.68	39.37 ± 0.72	74.63 ± 3.60
F6*	7:3	Tw 60	39.50 ± 3.1	305.6 ± 2.60	0.49 ± 0.023	−38.3 ± 1.2	50.83 ± 2.25	79.12 ± 1.66
F7*	9:1	Tw 20	52.60 ± 4.7	470.7 ± 5.20	0.46 ± 0.044	−31.6 ± 3.9	53.77 ± 2.70	83.36 ± 2.38
F8*	8:2	Tw 20	48.80 ± 3.3	324.5 ± 5.37	0.49 ± 0.034	−29.9 ± 1.7	58.98 ± 2.40	91.10 ± 2.03
F9*	7:3	Tw 20	22.45 ± 2.4	183.4 ± 2.76	0.38 ± 0.061	−32.3 ± 1.1	60.00 ± 1.33	94.10 ± 1.40

* All formulations contain 20 mg LF.

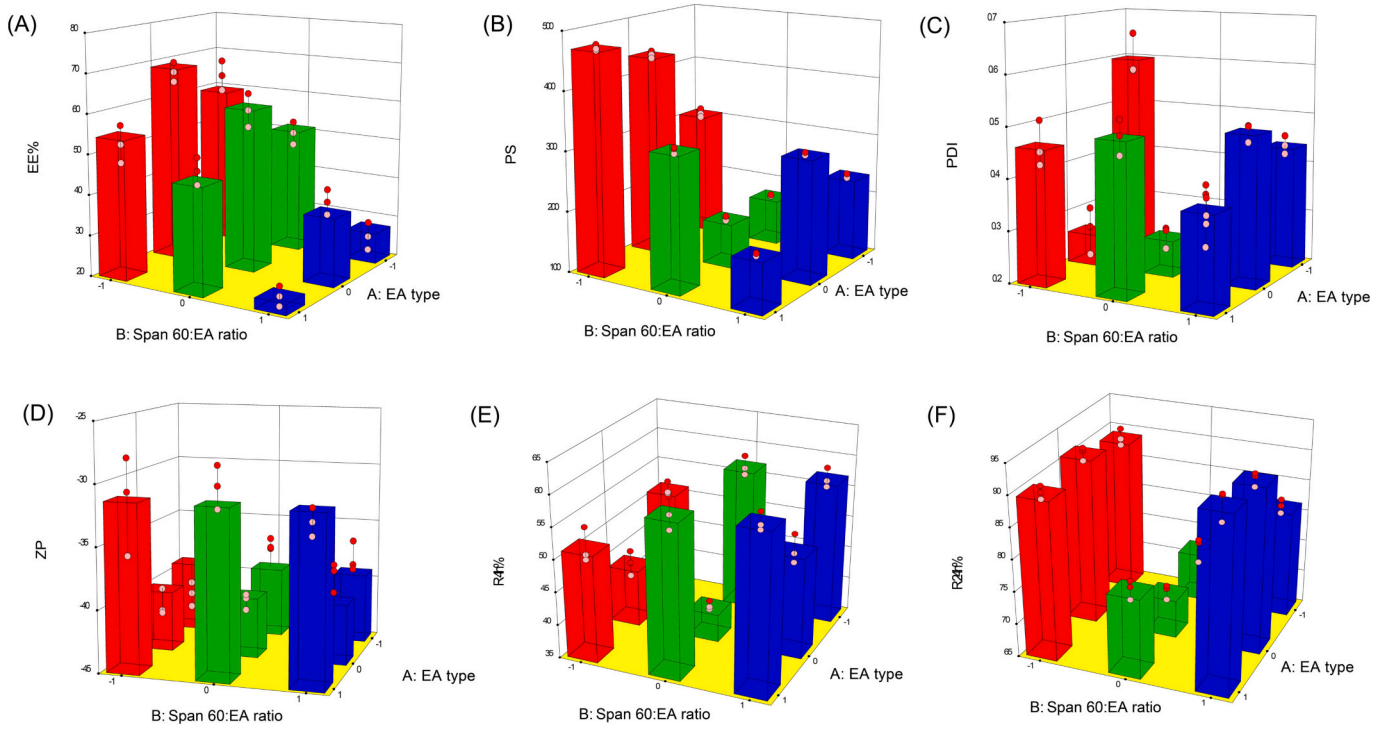

Fig. 1. Response 3-D plots for the effect of EA type (X1) and ratio of Span 60 to EA on (A) entrapment efficiency (EE %), (B) particle size (PS), (C) PDI, (D) zeta potential (ZP), (E) amount of LF released after 4 h ($R_{4h\%}$) and (F) amount of LF released after 24 h ($R_{24h\%}$).

Table 3
ANOVA results for the factorial analysis of responses.

Responses	F value	R^2	Adjusted R^2	Predicted R^2	Adequate Precision	Significant Factors
Y_1: EE%	91.28	0.948	0.938	0.905	23.62	X1, X_2
Y_2: PS (nm)	1811.31	0.999	0.998	0.997	104.87	X1, X_2
Y_3: PDI	36.31	0.948	0.922	0.851	17.33	X1, X_2
Y_4: ZP (mV)	40.43	0.786	0.767	0.678	10.27	X1
Y_5: R_{4h}%	40.03	0.952	0.929	0.865	17.45	X1, X_2
Y_6: R_{24h}%	94.95	0.979	0.969	0.941	22.90	X1, X_2

(lower HLB) would decrease the surface energy and form smaller particles and vice versa (ElMeshad and Mohsen, 2016; Yusuf et al., 2014). However Tween 80 and Tween 60 nearly have same HLP value, the unsaturated chain of Tween 80 could have enhanced the bending ability of the alky chain unlike the saturated alky chain of Tween 60 so produced smaller particles (Tayel et al., 2015). For X2, the amount of EA had negative effect on PS as increasing EA amount resulted in decreasing PS of the vesicles. This could be illustrated by the effect of EA on decreasing the interfacial tension and facilitating particles partition so give rise to smaller vesicles (Badria and Mazyed, 2020). Additionally, at high EA levels mixed micelles might be formed instead of vesicles, which possess smaller diameters (Basha et al., 2013).

PDI of all formulations ranged between 0.26 and 0.55 which is considered generally acceptable but PDI below 0.3 was preferred as some researchers suggested it as the accepted range for nano-carriers delivery systems. The low PDI value indicated a homogenous particles distribution and also revealed that SLs dispersion is stable as well as non-aggregated (Bin-Jumah et al., 2020).

4.1.3. Effect of formulation variables on ZP

ZP is a measure of all particles charge and values higher than ±30 are required to ensure system stability as a result of electrostatic repulsion force between vesicles that prevents particles agglomeration and enhancing stability (Abdelbary et al., 2016). In this design only X1 (Type of EA) had significant effect on ZP while X2 (EA amount) was insignificant. According to obtained data, ZP of all formulations was relatively high and ranged between −29.9 to −42.3 mV (Fig. 3B) where Tween 20 had the lowest values compared to both Tween 80 and 60. The imported negative charge to the particles could be caused by adsorbing OH^- ions of the dispersion media on particles membrane despite being nonionic surfactants (Soliman et al., 2016).

4.1.4. Effect of formulation variables on the LF% release

Fig. 6A below illustrates the release of LF from control solution and different SLs. It was obvious that incorporating LF within SL system significantly slowed down the drug release as the vesicular system is well-known to act as reservoir which slowly releases the drug providing sustained release profile (Ghanbarzadeh and Arami, 2013). The drug completely released from the solution within 4 h while SLs showed biphasic release state where about 39–60% was released rapidly in first 4 h due to surface-adsorbed free LF followed by sustained release from the vesicle core for about 24 h. This was in agreement with previous study (El Zaafarany et al., 2010). Analysis of the design data and statistics revealed that both EA type and amount (X1 and X2) had significant effect on the release profile but effect of X1 was much greater.

Regarding EA type (X1), SLs showed alky chain length dependent release as decreased alkyl chain of EA resulted in increased drug release where more fluidity imported to the bilayer membrane facilitating the drug release. In our model despite having the same hydrophilic head, the EA are differing in the hydrophobic alkyl chain so Tween 20 (with the smallest alkyl chain C = 12) provided higher release rate compared to Tween 60 and Tween 80 (C = 18) (Devaraj et al., 2002). Moreover, Tween 80 formulations showed faster release than Tween 60 due to alky chain unsaturation which might increase membrane fluidity and facilitate the drug leakage. According to EA concentration, X2 had positive effect on the release profile as faster release observed with increasing EAs amount which could increase the membrane fluidity and hence facilitate drug release so (7:3) ratio provided the highest release rate.

4.1.5. Release kinetics

Release kinetics of LF from prepared formulations is summarized in Table 4 below. All investigated formulations were best fitted into the Higuchi model with the optimum F5 displaying high r^2 value of 0.9947. Higuchi's model suggests that drug release occurs via diffusion through dispersed vesicles, and it proposes that the initial drug loading in the matrix exceeds its solubility in surrounding media thus results in a sink condition on the particles wall and allows the drug to be diffused in a constant and controlled manner in the release media (Paul, 2010).

Additionally, the Korsmeyer-Peppas model was found to be the most convenient model for analyzing the release of matrix-based systems. The Peppas model was applied to determine values of the release exponent (n) and found to be <0.5, indicating that the release profile of LF from investigated systems follows Fickian transport (Ritger and Peppas, 1987).

Table 4
Results of release kinetics of LF from investigated SLs.

Formula code	Correlation Coefficient (r^2)				Korsmeyer-peppas slope N
	Zero order	First order	Higuchi	Korsmeyer peppas	
F1	0.6336	0.9162	0.9573	0.9361	0.4387
F2	0.5764	0.8827	0.9222	0.9094	0.4278
F3	0.5905	0.8933	0.9332	0.9165	0.4255
F4	0.5871	0.8459	0.9499	0.9254	0.4016
F5	0.6586	0.8247	0.9947	0.9571	0.4089
F6	0.5670	0.7590	0.9667	0.9119	0.4115
F7	0.5681	0.7786	0.9492	0.9191	0.4021
F8	0.5623	0.8636	0.9319	0.8955	0.4431
F9	0.5641	0.9042	0.9259	0.9047	0.4207

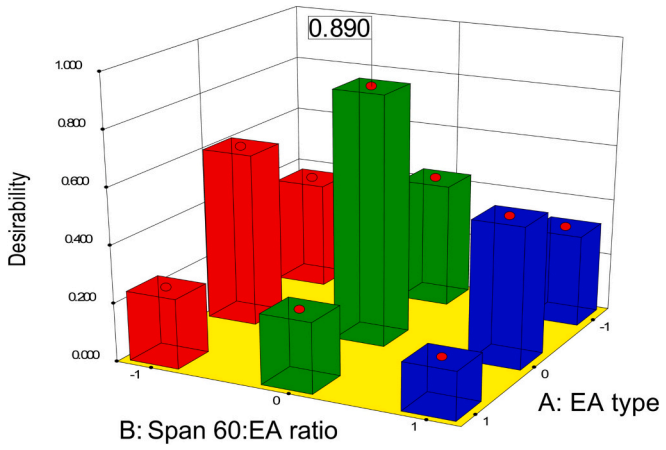

Fig. 2. Response 3-D plots for the effect of EA type (X1) and amount (X2) on desirability.

4.1.6. Determination of the Optimum SL Formulation

A complete factorial design using Design-Expert software was employed to analyze all measured responses of the prepared SLs formulations and determine the optimum formula. The selection criteria for the optimum formulation were to attain the highest EE% and ZP as absolute value while minimizing the values of PS and PDI. As shown in Fig. 2 below, F5 which was formulated with Tween 60 as an EA and Span 60: EA ratio (*w*/w) of 80:20, achieved the best criteria with a desirability of 0.89. Both the predicted and observed values of different responses of the optimum formulation are summarized in Table 5.

4.2. Characterization of the optimum LF-SL (F5)

4.2.1. Transmission electron microscopy (TEM)

The morphological examination of the optimum F5 is represented in Fig. 3C. It is exhibiting spherical shaped particles with well-defined walls, indicating its vesicular characteristics (ElMeshad and Mohsen, 2016). Also reveals the absence of vesicular aggregation, which may be attributed to the strong repulsive forces between the negatively charged particles (Tayel et al., 2015).

4.2.2. Solid state characterization

4.2.2.1. FT-IR Spectroscopy. FT-IR study was conducted to ensure components compatibility and absence of possible interactions between LF, Span 60 and EA (Tween 60). The FT-IR spectra of LF, Span 60, Tween 60, physical mixture and both plain and LF-loaded lyophilized SL (F5)

Table 5
Predicted and observed responses for optimized formulation F5.

	Responses	Predicted mean value	Observed experimental value	% RSD
Optimum formula coded (0,0)	Y_1: EE%	60.67	59.7 ± 4.2	1.6
	Y_2: PS (nm)	174	177.6 ± 1.8	2.07
	Y_3: PDI	0.27	0.27 ± 0.022	0
	Y_4: ZP (mV)	−40.03	−40.6 ± 0.68	1.4
	Y_5: R_{4h}%	39.35	39.37 ± 0.72	0.05
	Y_6: R_{24h}%	71.07	74.63 ± 3.6	5.01

% RSD equal to[(measured value-predicted value) / predicted value]× 100.

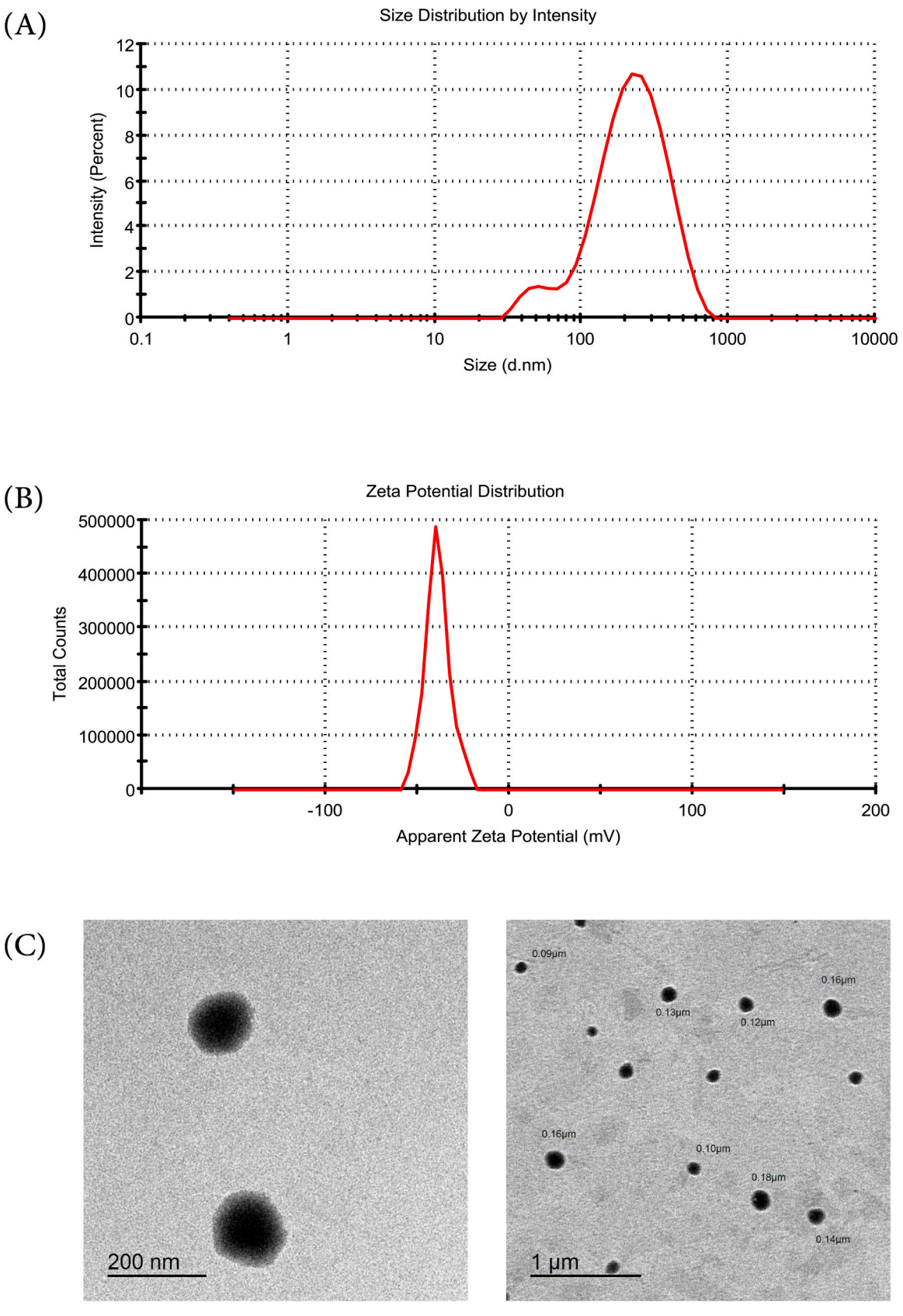

Fig. 3. Physicochemical characteristic of optimum F5, PS (A), ZP (B) and TEM analysis (C).

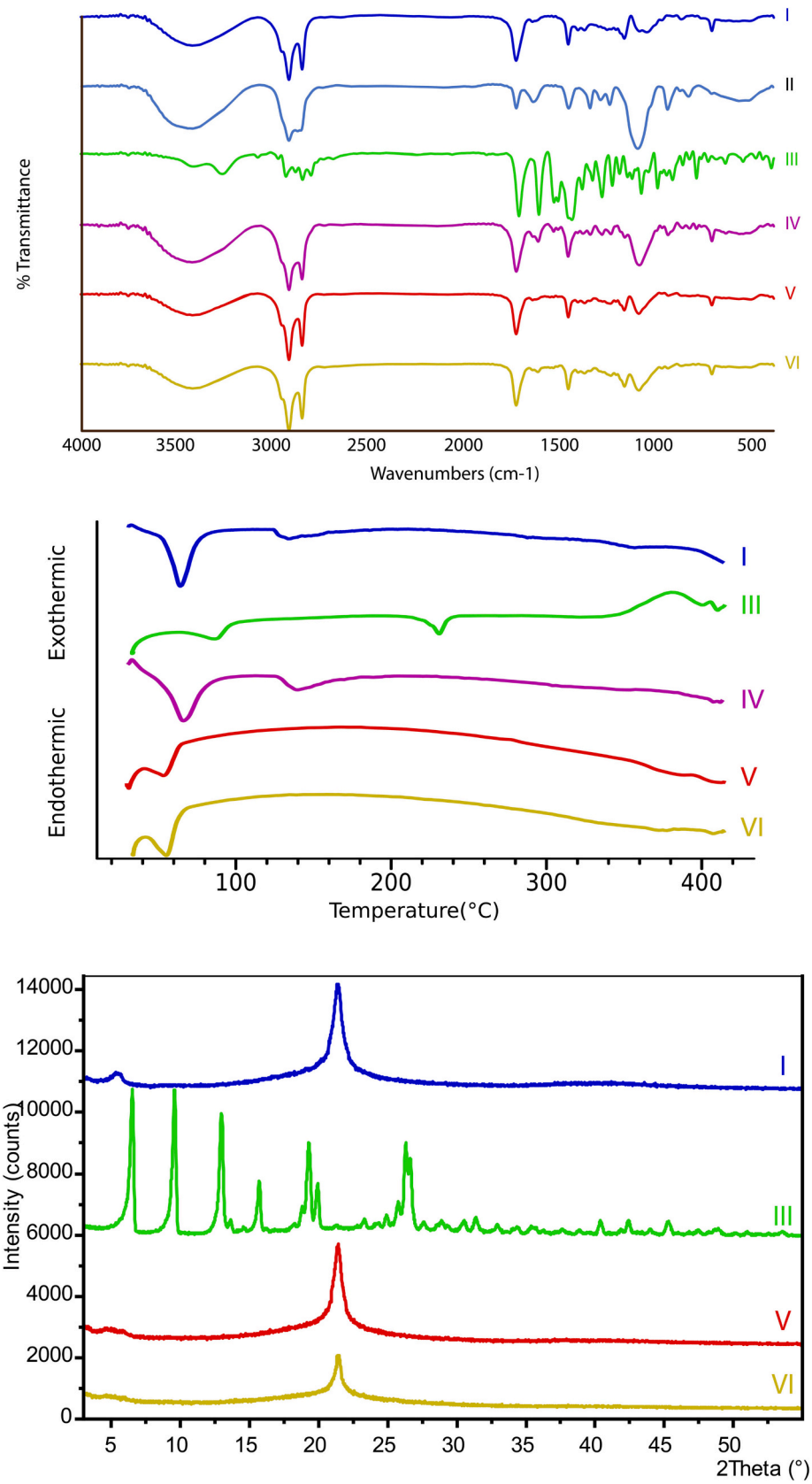

Fig. 4. Solid state characterization of optimum F5, FTIR (A), DSC (B) and XRD (C). Where I represents Span 60, II Tween 60, III free drug (LF), IV physical mixture, V plain F5 and VI medicated F5.

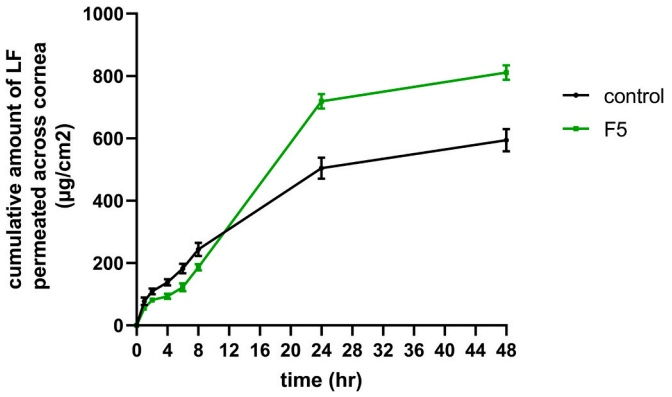

Fig. 5. Ex-vivo permeability study of LF across rabbit cornea from controlled solution and optimal spanlastic F5 (mean ± SD, $n = 3$).

Table 6
Characterization of prepared gelrite in situ gel (LSG).

Formula code	Gelrite conc *W/V*%	Gelling capacity	Viscosity (cp)		pH	Drug content (%)
			Before gelation	After gelation		
LSG1	0.1%	–	95.2	122	6.86 ± 0.12	98.57 ± 0.42
LSG2	0.2%	+	151.7	1593	6.97 ± 0.14	97.88 ± 0.95
LSG3	0.3%	++	248.4	5721	7.01 ± 0.13	98.73 ± 0.68
LSG4	0.4%	+++	684.6	9836	6.85 ± 0.09	97.04 ± 1.15
LSG5	0.5%	+++	2629	14,619	6.78 ± 0.15	96.91 ± 1.73

-, no gelation occur; +, spontaneous gelation but dissolves rapidly; ++, spontaneous gelation remains for few hours; +++, stiff gel forms instantly and remains for extended period.

are displayed in Fig. 4A. As shown in figure; FT-IR spectra of LF showed distinctive peaks at 3265 cm^{-1}(OH), 1620 cm^{-1}(C═O ring) and 1724 cm^{-1}(C═O acid) cm^{-1} as documented (Kugel et al., 2010), both Span 60 and Tween 60 shared common peaks at nearly 3420 cm^{-1}(OH), 2920, 2850 cm^{-1}(aliphatic CH stretching) and 1739 cm^{-1} (C═O strteching) (Farmoudeh et al., 2020). There was no suppression or appearance of additional peaks observed in spectra of F5 indicated no significant interaction between drug and other ingredients (Gupta et al., 2011).

4.2.2.2. Differential Scanning Calorimetry (DSC). Fig. 4B displays the DSC curves of LF, Span 60, their physical mixture, plain and LF-loaded F5. The thermogram of LF showed an endothermic peak at 87 °C due to the dehydration of LF, a melting endothermic peak at 231 °C that indicated crystallinity of pure LF (Ameeduzzafar Khan et al., 2020) and exothermic peak around 380 °C that might resulted from LF thermal degradation (Saher et al., 2016b) while Span 60 showed an endothermic peak at around 60 °C (Mady et al., 2019). The distinctive sharp peak of Span 60 was visible in thermogram of the physical mixture while that of drug couldn't be distinguished due to dilution effect (Mohamed et al., 2017).

There was a slight shift in the peak of Span 60 from 64 to 54 °C in both plain and medicated F5 that could be due to assembly of Span 60 into the SLs bilayers that decreased its fusion point (El-Ridy et al., 2011) (AbuElfadl et al., 2021). However the peaks of drug were completely disappeared in both plain and medicated thermograms which indicated a complete encapsulation of drug and its conversion to amorphous form instead of the crystalline drug form (Mohamed et al., 2017) (Zafar et al., 2022). As conclusion, the DSC thermogram eliminated any incompatibility among the system components.

4.2.2.3. X-ray Diffractometry (XRD). Diffractogram of LF, Span 60, physical mixture in addition to both plain and LF-loaded F5 is represented in Fig. 4C. As well as DSC, also XRD used to study the incompatibility between various system components and monitoring the physical state of the drug. From the graph, it is clear that the distinctive peak corresponding to pure LF was completely disappeared in case of F5 which clarified complete entrapment of the drug within the vesicular system and its conversion from the crystalline pure state to an amorphous state, which in consistent with the findings of the DSC study (Gupta et al., 2011).

4.3. Corneal permeability study

Fig. 5 below represents the cumulative amount of LF permeated across the cornea from both F5 and LS solution as control over 48 h. From results, SLs demonstrated a significant ($p<0.05$) enhancement in LF apparent permeation coefficient (Papp) (14.7×10^{-3} cm/h) in

Table 7
Results of in-vitro microbiological study.

MIC(µg/mL)			MBC(µg/mL)	
Strain	*Pseudomonas aeruginosa*	*Staphylococcus aureus*	*Pseudomonas aeruginosa*	*Staphylococcus aureus*
control	1	0.25	2	0.5
F5	0.25	0.125	0.5	0.125
Plain F5	No activity	No activity	–	–

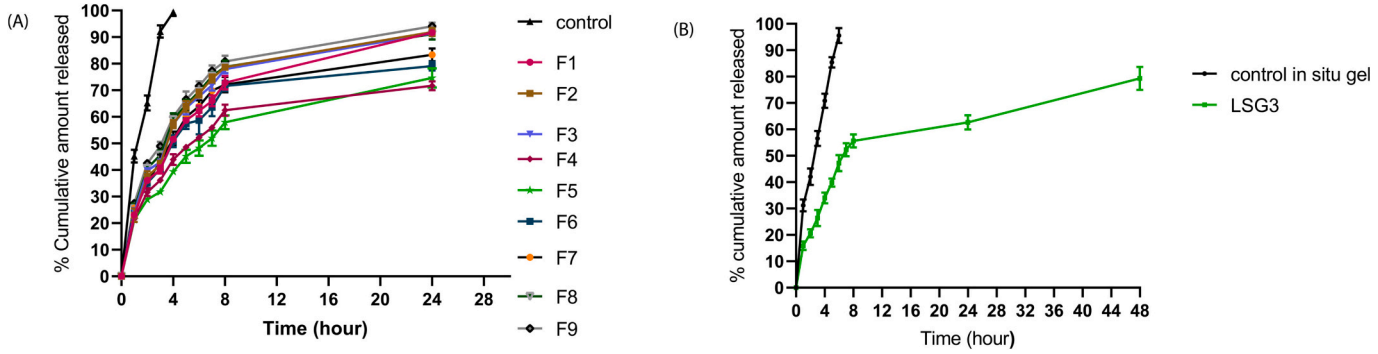

Fig. 6. In-vitro drug release of LF from (A) optimum SLs (F5) and (B) optimum spanlastic laden in-situ gel (LSG3)eye in comparison with LF solution and LF in-situ gel in STF (pH = 7.4) at 37 ± 0.5 °C (mean ± SD, n = 3).

Table 8
Effect of the different storage conditions on the physicochemical properties of F5. Each value represents the mean ± SD ($n = 3$).

F5	Zero time	First month		Second month		Third month	
		T = 4 °c	T = 25 °c	*T* = 4 °c	*T* = 25 °c	T = 4°c	T = 25 °c
EE%	59.3 ± 5.5	57.4 ± 4.2	55.9 ± 3.9	57.3 ± 6.8	53.7 ± 4.04	55.2 ± 4.6	52.5 ± 5.6
PS	175.6 ± 3.8	171 ± 3.1	166.6 ± 2.8	179.8 ± 4.1	167.1 ± 4.9	174 ± 2.6	214.4 ± 0.6
PDI	0.24 ± 0.01	0.23 ± 0.02	0.24 ± 0.01	0.24 ± 0.03	0.24 ± 0.01	0.25 ± 0.01	0.2 ± 0.01
ZP	−39.8 ± 1.7	−36.5 ± 1.4	−32.1 ± 0.7	−42.1 ± 1.4	−32.5 ± 0.35	−37.6 ± 1.7	−28.4 ± 1.3

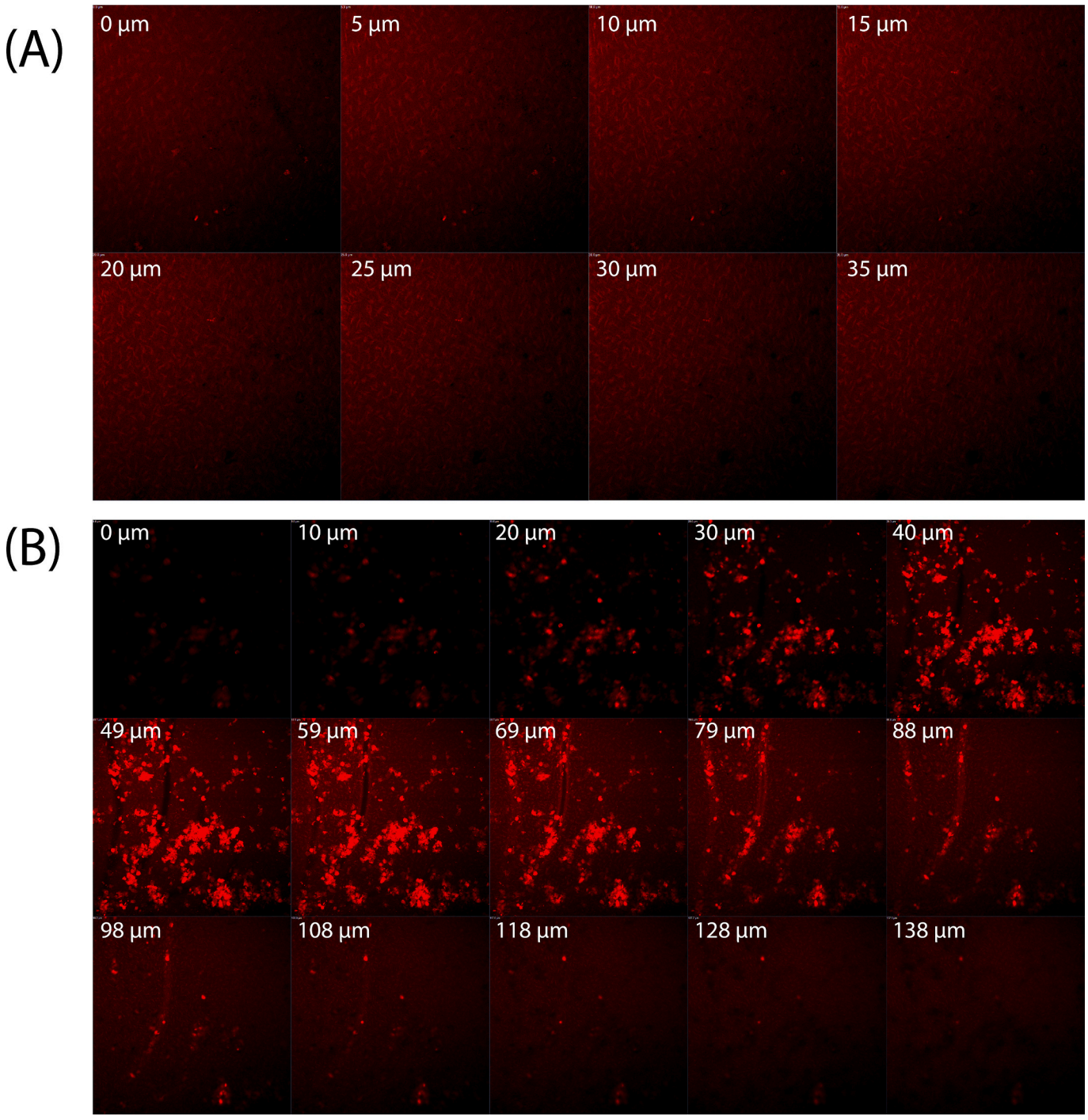

Fig. 7. Comparative confocal laser scanning microscopy images show depth and intensity of Rhodamine B solution (A) and Rhodamine incorporated in optimum SL (B) penetration across the corneal tissue.

comparison to LF solution (9.7×10^{-3} cm/h). Additionally, there was a significant difference in terms of the total amount of LF permeated through rabbit cornea after 48 h, with 636.81 ± 18.28 μg for F5 and only 466.23 ± 27.78 μg for LF solution. This could be attributed to the presence of surfactants (span 60 and EA) in the SLs, which could increase the endocytosis through the corneal epithelium and leads to greater permeation across the membrane (Gilani et al., 2022). Consequently, it could be concluded that SPs, as a vesicular system, significantly enhanced the corneal penetration of LF over the conventional solution.

4.4. Formulation and characterization of LSG

Table 6 below presents the results of different characteristics of the prepared LSGs. The gelling capacity of the investigated solutions was directly proportional to gelrite concentration and divided into 4 groups (Almajidi et al., 2019). The pH of all formualtions ranged from 6.78 ± 0.15 to 7.01 ± 0.13, which is considered suitable for ocular application. The drug content was within a reasonable percentage. Based to the obtained results, 0.3 *w/v*% gelrite was selected as the optimum concentration for incorporating (F5) as it provided suitable gel that formed instantly and remained intact for up to 6 h with an accepted viscosity.

Fig. 6B represents LF in-vitro release profile from LSG3 compared to free LF in situ gel. LSG3 provided extended release over both LF gel and F5 which proves the dual action of incorporating the vesicular system within gel.

4.5. Microbiological study of optimum F5

The in-vitro antibacterial activity of free LF, LF Loaded F5 loaded, and plain F5 was appraised by determining MIC and MBC values against both *Pseudomonas aeruginosa* (gram+) and *Staphylococcus aureus* (gram-) bacteria. As presented in Table 7, MIC values indicated that plain F5 exhibited no activity, while LF-loaded F5 was a four-fold and two-fold increase in activity against *Pseudomonas aeruginosa* and *Staphylococcus aureus* respectively. Furthermore, the MBC values indicated 400% increase in bactericidal activity against both strains compared to the marketed product. These results provide evidence for the role of SL vesicular system in enhancement of the antibacterial activity of LF.

4.6. Stability study

Following three months of storage, the optimum formula F5 exhibited no changes in appearance when stored under different storage conditions. The study of %EE, PS, PDI and ZP played a crucial role in monitoring the system's stability. As illustrated in Table 8, at −4 °c there was insignificant change ($\rho < 0.05$) in the EE%, PS, PDI or ZP of F5 throughout the study period, indicating good stability compared to the freshly prepared formulation. The physical stability observed in F5 at −4 °C might be attributed to the presence of the vesicular bilayer in the solid state at refrigeration temperature, which could prevent drug leakage from the vesicles. Additionally, the high zeta potential may have hindered the aggregation and fusion of vesicles during storage as reported beforre (Farghaly et al., 2017). However, a slight change in the ZP of F5 was observed when stored at 25 °c. Therefore, it's recommended to be stored in a refrigerator at −4 °C.

4.7. In-vivo study

4.7.1. Eye irritation test

Animals' right eye was examined at time intervals and compared to the left control one. No signs of irritation or congestion appeared after formulations application. That's indicated safety of the formulations on the eye tissue and hence they can be used for ocular drug delivery.

4.7.2. Corneal penetration study by CLSM

The in-vivo model was preferred over the ex-vivo study to simulate the natural physiological process for conducting the CLSM study. Fig. 7 shows a series of optical sections captured at different focal planes along the z-axis to provide three-dimensional details about the penetration of RhB from either the solution or RhB-loaded SL across the corneal tissue.

From the images in Fig. 7, it is obvious that there was a significant difference in both the depth and intensity of RhB fluorescence between the solution and SL. In case of the solution, fluorescence could be detected only at a depth of 35 μm, while in the case of SL, fluorescence still could be observed up to 137 μm which considered about 300% increase in the penetration ability. Regarding the intensity, for SL, there was a gradual increase in fluorescence intensity from superficial layers to lower ones till maximum intensity after which it started to decrease till completely vanished. Conversely, for the solution, only a minimal amount could penetrate which was responsible for tiny fluorescence observed. This could be attributed to the rapid drainage of RhB solution from the eye surface after topical application, which limits the availability of the drug for penetration. On the other hand, SL acted as a depot that was stucked in tissues and gradually releasing RhB over time.

5. Conclusion

Based on the study results, it was found that SLs could be a promising vesicular system for enhancing and sustaining the ocular delivery of the antibacterial drug LF. The optimal formulation exhibited small PS, appropriate ZP, relatively high drug EE%, and spherical morphology. The release of LF from the system was sustained for up to 24 h in comparison to the conventional drug solution. Incorporating the optimum F5 within gelrite in situ gel provided a dual effect in sustaining drug release and increasing the corneal retention time thanks to the gel's mucoadhesive properties. Thus could overcome the need for repeated dosing every 2 h.

The nano-vesicular system also increased the drug permeation across the rabbit cornea about 1.5 fold compared to the drug solution. The in-vitro antibacterial study revealed 100–200% enhancement in drug activity against tested organisms when incorporated within SLs, as compared to the marketed product. The CLSM was conducted and confirmed the results of the in-vitro corneal permeability study. Significantly higher fluorescence intensity was detected in deeper corneal layers in case of SL upon comparison to RhB solution.

The system stability was maintained upon storage in a refrigerator for up to 3 months. Finally, an in-vivo safety study was performed and revealed the suitability of the formulation for ocular application without any undesirable effects. Based on these findings, it can be concluded that SL laden in situ gel can be employed for promoting corneal delivery of LF in topical antibacterial treatment surpassing traditional marketed eyedrops.

Credit author statement

Omnia Ahmed Agha: conceptualization, data collection, methodology, investigation, formal analysis and interpretation of results, writing and editing final manuscript.

Germeen N S Girgis: conceptualization, data collection, analysis, supervision, and revising manuscript.

Mohamed M A El-Sokkary: conducting the in vitro antibacterial study, analyzing obtained data and writing results.

Osama Abd El-Azeem Soliman: conceptualization, supervision, reviewing and editing manuscript.

Declaration of Competing Interest

The authors declare that they have no conflicts of interest to disclose and the research did not receive any specific grant from funding agencies in the public, commercial, or not-for-profit sectors.

Data availability

Data will be made available on request.

References

Abdelbari, M.A., El-Mancy, S.S., Elshafeey, A.H., Abdelbary, A.A., 2021. Implementing spanlastics for improving the ocular delivery of clotrimazole: in vitro characterization, ex vivo permeability, microbiological assessment and in vivo safety study. Int. J. Nanomedicine 16, 6249–6261. https://doi.org/10.2147/IJN.S319348.

Abdelbary, A.A., Abd-Elsalam, W.H., Al-Mahallawi, A.M., 2016. Fabrication of novel ultradeformable bilosomes for enhanced ocular delivery of terconazole: in vitro characterization, ex vivo permeation and in vivo safety assessment. Int. J. Pharm. 513, 688–696. https://doi.org/10.1016/j.ijpharm.2016.10.006.

Abdelrahman, A.A., Salem, H.F., Khallaf, R.A., Ali, A.M.A., 2015. Modeling, optimization, and in vitro corneal permeation of chitosan-lomefloxacin HCl nanosuspension intended for ophthalmic delivery. J. Pharm. Innov. 10, 254–268. https://doi.org/10.1007/s12247-015-9224-7.

AbuElfadl, A., Boughdady, M., Meshali, M., 2021. New PeceolTM/SpanTM 60 niosomes coated with chitosan for candesartan cilexetil: perspective increase in absolute bioavailability in rats. Int. J. Nanomedicine 16, 5581–5601. https://doi.org/10.2147/IJN.S324171.

Al-Mahallawi, A.M., Khowessah, O.M., Shoukri, R.A., 2017. Enhanced non invasive trans-tympanic delivery of ciprofloxacin through encapsulation into nano-spanlastic vesicles: Fabrication, in-vitro characterization, and comparative ex-vivo permeation studies. Int. J. Pharm. 522, 157–164. https://doi.org/10.1016/j.ijpharm.2017.03.005.

Almajidi, Q., Albaderi, A., Fadhel, H., 2019. Enhance solubility and prolong release of prochlorperazine maleate using floating nanoemulsion in situ gel. Asian J Pharm Clin Res. 12, 537–541. https://doi.org/10.22159/ajpcr.2019.v12i1.30486.

Alsaidan, O.A., Zafar, A., Yasir, M., Alzarea, S.I., Alqinyah, M., Khalid, M., 2022. Development of ciprofloxacin-loaded bilosomes in-situ gel for ocular delivery: optimization, in-vitro characterization, ex-vivo permeation, and antimicrobial study. Gels. 8, 687. https://doi.org/10.3390/gels8110687.

Ameeduzzafar Imam, S.S., Abbas Bukhari, S.N., Ahmad, J., Ali, A., 2018. Formulation and optimization of levofloxacin loaded chitosan nanoparticle for ocular delivery: in-vitro characterization, ocular tolerance and antibacterial activity. Int. J. Biol. Macromol. 108, 650–659. https://doi.org/10.1016/j.ijbiomac.2017.11.170.

Ameeduzzafar Khan, N., Alruwaili, N.K., Bukhari, S.N.A., Alsuwayt, B., Afzal, M., Akhter, S., Yasir, M., Elmowafy, M., Shalaby, K., Ali, A., 2020. Improvement of ocular efficacy of levofloxacin by bioadhesive chitosan coated plga nanoparticles: box-behnken design, *in-vitro* characterization, antibacterial evaluation and scintigraphy study. Iran J Pharm Res. 19, 292–311. https://doi.org/10.22037/ijpr.2019.15318.13016.

Araújo, J., Gonzalez-Mira, E., Egea, M.A., Garcia, M.L., Souto, E.B., 2010. Optimization and physicochemical characterization of a triamcinolone acetonide-loaded NLC for ocular antiangiogenic applications. Int. J. Pharm. 393, 167–175. https://doi.org/10.1016/j.ijpharm.2010.03.034.

Badria, F., Mazyed, E., 2020. Formulation of nanospanlastics as a promising approach for improving the topical delivery of a natural leukotriene inhibitor (3-acetyl-11-Keto-β-boswellic acid): statistical optimization, in vitro characterization, and ex vivo permeation study. Drug Des Devel Ther. 14, 3697–3721. https://doi.org/10.2147/DDDT.S265167.

Baig, M.S., Ahad, A., Aslam, M., Imam, S.S., Aqil, M., Ali, A., 2016. Application of Box-Behnken design for preparation of levofloxacin-loaded stearic acid solid lipid nanoparticles for ocular delivery: optimization, in vitro release, ocular tolerance, and antibacterial activity. Int. J. Biol. Macromol. 85, 258–270. https://doi.org/10.1016/j.ijbiomac.2015.12.077.

Basha, M., Abd El-Alim, S.H., Shamma, R.N., Awad, G.E., 2013. Design and optimization of surfactant-based nanovesicles for ocular delivery of clotrimazole. J Liposome Res. 23, 203–210. https://doi.org/10.3109/08982104.2013.788025.

Bin-Jumah, M., Gilani, S.J., Jahangir, M.A., Zafar, A., Alshehri, S., Yasir, M., Kala, C., Taleuzzaman, M., Imam, S.S., 2020. Clarithromycin-loaded ocular chitosan nanoparticle: formulation, optimization, characterization, ocular irritation, and antimicrobial activity. Int. J. Nanomedicine 15, 7861–7875. https://doi.org/10.2147/IJN.S269004.

Bourlais, C.L., Acar, L., Zia, H., Sado, P.A., Needham, T., Leverge, R., 1998. Ophthalmic drug delivery systems–recent advances. Prog. Retin. Eye Res. 17, 33–58. https://doi.org/10.1016/s1350-9462(97)00002-5.

De Gaetano, F., Marino, A., Marchetta, A., Bongiorno, C., Zagami, R., Cristiano, M.C., Paolino, D., Pistarà, V., Ventura, C.A., 2021. Development of chitosan/cyclodextrin nanospheres for levofloxacin ocular delivery. Pharmaceutics. 13, 1293. https://doi.org/10.3390/pharmaceutics13081293.

Devaraj, G.N., Parakh, S.R., Devraj, R., Apte, S.S., Rao, B.R., Rambhau, D., 2002. Release studies on niosomes containing fatty alcohols as bilayer stabilizers instead of cholesterol. J. Colloid Interface Sci. 251, 360–365. https://doi.org/10.1006/jcis.2002.8399.

Dhangar, R., Bhowmick, M., Parihar, S.S., Upmanyu, N., Dubey, B., 2014. Design and evaluation of proniosomes as drug carrier for ocular delivery of levofloxacin. J Drug Deliv Therapeut. 4, 182–189. https://doi.org/10.22270/jddt.v4i5.740.

Draize, J.H., Woodard, G., Calvery, H.O., 1944. Methods for the study of irritation and toxicity of substances applied topically to the skin and mucous membranes. J. Pharmacol. Exp. Ther. 82, 377–390.

Duangjit, S., Opanasopit, P., Rojanarata, T., Ngawhirunpat, T., 2011. Characterization and in vitro skin permeation of meloxicam-loaded liposomes versus transfersomes. J Drug Deliv. 2011, 418316 https://doi.org/10.1155/2011/418316.

El Zaafarany, G.M., Awad, G.A., Holayel, S.M., Mortada, N.D., 2010. Role of edge activators and surface charge in developing ultradeformable vesicles with enhanced skin delivery. Int. J. Pharm. 397, 164–172. https://doi.org/10.1016/j.ijpharm.2010.06.034.

Elmeshad, A.N., Mohsen, A.M., 2016. Enhanced corneal permeation and antimycotic activity of itraconazole against Candida albicans via a novel nanosystem vesicle. Drug Deliv. 23, 2115–2123. https://doi.org/10.3109/10717544.2014.942811.

El-Ridy, M.S., Abdelbary, A., Essam, T., El-Salam, R.M., Kassem, A.A., 2011. Niosomes as a potential drug delivery system for increasing the efficacy and safety of nystatin. Drug Dev. Ind. Pharm. 37, 1491–1508. https://doi.org/10.3109/03639045.2011.587431.

Elsayed, I., Sayed, S., 2017. Tailored nanostructured platforms for boosting transcorneal permeation: Box–Behnken statistical optimization, comprehensive in vitro, ex vivo and in vivo characterization. Int. J. Nanomedicine 12, 7947–7962. https://doi.org/10.2147/IJN.S150366.

Farghaly, D.A., Aboelwafa, A.A., Hamza, M.Y., Mohamed, M.I., 2017. Topical delivery of fenoprofen calcium via elastic nano-vesicular spanlastics: optimization using experimental design and in vivo evaluation. AAPS PharmSciTech 18, 2898–2909. https://doi.org/10.1208/s12249-017-0771-8.

Farmoudeh, A., Akbari, J., Saeedi, M., Ghasemi, M., Asemi, N., Nokhodchi, A., 2020. Methylene blue-loaded niosome: preparation, physicochemical characterization, and in vivo wound healing assessment. Drug Deliv Transl Res. 10, 1428–1441. https://doi.org/10.1007/s13346-020-00715-6.

Ghanbarzadeh, S., Arami, S., 2013. Enhanced transdermal delivery of diclofenac sodium via conventional liposomes, ethosomes, and transfersomes. Biomed. Res. Int. 2013, 616810 https://doi.org/10.1155/2013/616810.

Gilani, S.J., Jumah, M.N.B., Zafar, A., Imam, S.S., Yasir, M., Khalid, M., Alshehri, S., Ghuneim, M.M., Albohairy, F.M., 2022. Formulation and evaluation of nano lipid carrier-based ocular gel system: optimization to antibacterial activity. Gels. 8, 255. https://doi.org/10.3390/gels8050255.

Guinedi, A.S., Mortada, N.D., Mansour, S., Hathout, R.M., 2005. Preparation and evaluation of reverse-phase evaporation and multilamellar niosomes as ophthalmic carriers of acetazolamide. Int. J. Pharm. 306, 71–82. https://doi.org/10.1016/j.ijpharm.2005.09.023.

Gupta, H., Aqil, M., Khar, R.K., Ali, A., Bhatnagar, A., Mittal, G., 2011. Biodegradable levofloxacin nanoparticles for sustained ocular drug delivery. J. Drug Target. 19, 409–417. https://doi.org/10.3109/1061186X.2010.504268.

Higuchi, T., 1963. Mechanism of sustained-action medication. theoretical analysis of rate of release of solid drugs dispersed in solid matrices. J. Pharm. Sci. 52, 1145–1149. https://doi.org/10.1002/jps.2600521210.

Hooper, D.C., 1999. Mode of action of fluoroquinolones. Drugs. 58, 6–10. https://doi.org/10.2165/00003495-199958002-00002.

Janoria, K.G., Gunda, S., Boddu, S.H., Mitra, A.K., 2007. Novel approaches to retinal drug delivery. Expert Opin Drug Deliv. 4, 371–388. https://doi.org/10.1517/17425247.4.4.371.

Kahlmeter, G., Brown, D.F., Goldstein, F.W., MacGowan, A.P., Mouton, J.W., Osterlund, A., Rodloff, A., Steinbakk, M., Urbaskova, P., Vatopoulos, A., 2003. European harmonization of MIC breakpoints for antimicrobial susceptibility testing of bacteria. J. Antimicrob. Chemother. 52, 145–148. https://doi.org/10.1093/jac/dkg312.

Kakkar, S., Kaur, I.P., 2011. Spanlastics–a novel nanovesicular carrier system for ocular delivery. Int. J. Pharm. 413, 202–210. https://doi.org/10.1016/j.ijpharm.2011.04.027.

Korsmeyer, R.W., Gurny, R., Doelker, E., Buri, P., Peppas, N.A., 1983. Mechanisms of solute release from porous hydrophilic polymers. Int. J. Pharm. 15, 25–35. https://doi.org/10.1016/0378-5173(83)90064-9.

Kugel, A., Chisholm, B., Ebert, S., Jepperson, M., Jarabek, L., Stafslien, S., 2010. Antimicrobial polysiloxane polymers and coatings containing pendant levofloxacin. Polym. Chem. 1, 442–452. https://doi.org/10.1039/B9PY00309F.

Kumar, S., Haglund, B.O., Himmelstein, K.J., 1994. In situ-forming gels for ophthalmic drug delivery. J. Ocul. Pharmacol. 10, 47–56. https://doi.org/10.1089/jop.1994.10.47.

Mady, O.Y., Donia, A.A., Al-Shoubki, A.A., Qasim, W., 2019. Paracellular pathway enhancement of metformin hydrochloride *via* molecular dispersion in span 60 microparticles. Front. Pharmacol. 10, 713. https://doi.org/10.3389/fphar.2019.00713.

Martin, A.N., Bustamante, P., Chun, A.H.C., 1993. Physical Pharmacy : Physical Chemical Principles in the Pharmaceutical Sciences, fourth ed. Lea & Febiger, Philadelphia (Pa.).

Mehanna, M.M., Mneimneh, A.T., Abed El Jalil, K., 2020. Levofloxacin-loaded naturally occurring monoterpene-based nanoemulgel: a feasible efficient system to circumvent MRSA ocular infections. Drug Dev. Ind. Pharm. 46, 1787–1799. https://doi.org/10.1080/03639045.2020.1821048.

Moawad, F.A., Ali, A.A., Salem, H.F., 2017. Nanotransfersomes-loaded thermosensitive in situ gel as a rectal delivery system of tizanidine HCl: preparation, in vitro and in vivo performance. Drug Deliv. 24, 252–260. https://doi.org/10.1080/10717544.2016.1245369.

Mohamed, H.B., El-Shanawany, S.M., Hamad, M.A., Elsabahy, M., 2017. Niosomes: A strategy toward Prevention of Clinically significant Drug Incompatibilities. Sci. Rep. 7, 6340. https://doi.org/10.1038/s41598-017-06955-w.

Noel, G., 2009. A review of levofloxacin for the treatment of bacterial infections. Clin. Med. Therapeut. 1 https://doi.org/10.4137/CMT.S28.

Paul, D.R., 2010. Elaborations on the Higuchi model for drug delivery. Int. J. Pharm. 418, 13–17. https://doi.org/10.1016/j.ijpharm.2010.10.037.

Ritger, P.L., Peppas, N.A., 1987. A simple equation for description of solute release II. Fickian and anomalous release from swellable devices. J. Control. Release 5, 37–42. https://doi.org/10.1016/0168-3659(87)90035-6.

Saher, O., Ghorab, D.M., Mursi, N.M., 2016a. Levofloxacin hemihydrate ocular semi-sponges for topical treatment of bacterial conjunctivitis: Formulation and in-vitro/in-vivo characterization. J Drug Deliv Sci Technol. 31, 22–34. https://doi.org/10.1016/j.jddst.2015.11.004.

Saher, O., Ghorab, D.M., Mursi, N.M., 2016b. Preparation and in vitro/in vivo evaluation of antimicrobial ocular in situ gels containing a disappearing preservative for topical treatment of bacterial conjunctivitis. Pharm. Dev. Technol. 21, 600–610. https://doi.org/10.3109/10837450.2015.1035728.

Sayed, S., Abdelmoteleb, M., Amin, M.M., Khowessah, O.M., 2020. Effect of formulation variables and gamma sterilization on transcorneal permeation and stability of proniosomal gels as ocular platforms for antiglaucomal drug. AAPS PharmSciTech 21, 87. https://doi.org/10.1208/s12249-020-1626-2.

Shamma, R.N., Elsayed, I., 2013. Transfersomal lyophilized gel of buspirone HCl: formulation, evaluation and statistical optimization. J Liposome Res. 23, 244–254. https://doi.org/10.3109/08982104.2013.801489.

Singh, M., Guzman-Aranguez, A., Hussain, A., Srinivas, C.S., Kaur, I.P., 2019. Solid lipid nanoparticles for ocular delivery of isoniazid: evaluation, proof of concept and in vivo safety & kinetics. Nanomedicine (London) 14, 465–491. https://doi.org/10.2217/nnm-2018-0278.

Soliman, S.M., Abdelmalak, N.S., El-Gazayerly, O.N., Abdelaziz, N., 2016. Novel non-ionic surfactant proniosomes for transdermal delivery of lacidipine: optimization using 2(3) factorial design and in vivo evaluation in rabbits. Drug Deliv. 23, 1608–1622. https://doi.org/10.3109/10717544.2015.1132797.

Tayel, S.A., El-Nabarawi, M.A., Tadros, M.I., Abd-Elsalam, W.H., 2015. Duodenum-triggered delivery of pravastatin sodium via enteric surface-coated nanovesicular spanlastic dispersions: development, characterization and pharmacokinetic assessments. Int. J. Pharm. 483, 77–88. https://doi.org/10.1016/j.ijpharm.2015.02.012.

Yoncheva, K., Lizarraga, E., Irache, J.M., 2005. Pegylated nanoparticles based on poly (methyl vinyl ether-co-maleic anhydride): preparation and evaluation of their bioadhesive properties. Eur. J. Pharm. Sci. 24, 411–419. https://doi.org/10.1016/j.ejps.2004.12.002.

Yusuf, M., Sharma, V., Pathak, K., 2014. Nanovesicles for transdermal delivery of felodipine: development, characterization, and pharmacokinetics. Int J Pharm Investig. 4, 119–130. https://doi.org/10.4103/2230-973X.138342.

Zafar, A., Alsaidan, O.A., Imam, S.S., Yasir, M., Alharbi, K.S., Khalid, M., 2022. Formulation and Evaluation of Moxifloxacin Loaded Bilosomes In-Situ Gel: Optimization to Antibacterial Evaluation. Gels. 8, 418. https://doi.org/10.3390/gels8070418.